Oleylamine-Stabilized Gold Nanostructures for Bioelectronic Assembly. Direct Electrochemistry of Cytochrome *c*.

Ekaterina Koposova,[§] Alexandre Kisner[&], Galina Shumilova,[§] Yury Ermolenko,[§] Andreas Offenhäusser, [&] and Yulia Mourzina[*,&]*

[§]Faculty of Chemistry, St. Petersburg State University, Universitetskaya nab. 7/9, 199034 St. Petersburg, Russia, and [&]Peter-Grünberg Institute-8, Forschungszentrum Jülich GmbH, 52428, Jülich and Jülich-Aachen Research Alliance - Fundamentals of Future Information Technology (JARA-FIT)

Corresponding Author:

Dr. Yulia Mourzina

Peter-Grünberg Institute-8, Forschungszentrum Jülich GmbH, 52428, Jülich and Jülich-Aachen Research Alliance (JARA_FIT). Tel: +49 2461612364; Fax: +49 2461618733; E-mail: y.mourzina@fz-juelich.de

The work was conducted in the Peter-Grünberg Institute-8, Forschungszentrum Jülich GmbH, 52428, Jülich and Jülich-Aachen Research Alliance (JARA-FIT).

ABSTRACT. Methods to prepare ultrathin gold nanowires and monodisperse nanoparticles based on the intrinsic property of gold (I) ions to form aurophilic interactions stabilized by oleylamine and long-chain alkylamine have been widely explored. Due to the low thermodynamic stability of the high aspect ratio nanostructures, their conjugation and assembly into functional nanosystems have not been explored so far. One of the reasons for this is that the surface of the nanostructures is insulated by stabilization compounds, which preserve the integrity of the nanostructures but at the same time, form an insulating barrier in electronic and electrochemical systems in contact areas and for the charge transfer reactions. Conjugation of a metalloprotein cytochrome *c* (Cyt *c*) with oleylamine-stabilized gold ultrathin nanowires and nanoparticles into a bioelectrochemically active nanoarchitecture is presented here for the first time. Methods of preparing and assembling the ultrathin nanowires and nanoparticles on the thin film gold electrodes are shown. Thermodynamic and kinetic parameters were obtained for the direct electron transfer reaction of cyt *c* on these surfaces. Nanowires are responsible for an approximately -20 mV shift in the redox potential of the ferri/ferro-cyt *c* couple relative to a thin film gold electrode.

Keywords: Metaloprotein, Nanowires, Nanoparticles, Cyclic voltammetry, Electron transfer,

Self-assembled monolayer

1. Introduction

Cytochrome *c* (Cyt *c*) is one of the most extensively studied proteins because of its central role in electron transfer in living organisms and as a consequence of electron shuttle between molecular partners in artificial bioelectronic systems.[1,2] Conjugation of cyt *c* with nanoelectronic elements may provide an opportunity to develop platforms with new and unique properties with respect to electron transfer rate, potential range as well as amount of immobilized electroactive metalloprotein. Conjugation of electroactive cyt *c* with nanostructured materials has been reported.[3-6] Recently, an inexpensive and versatile synthesis for producing various gold nanostructures employing oleylamine (OA) as a reducing agent and stabilizer has been studied by different authors.[7-12] Ultrathin nanowires 2 nm in diameter and with an aspect ratio of up to 4000 have been obtained by this method.[8] The nanowires present a face-centered cubic crystalline structure and thus have about 70% of the atoms on their surface, suggesting that these new metallic nanostructures could be used to design new electrochemical platforms with a large surface area. Although this method has been widely used, the nanostructures (NS) prepared so far have not been exploited for electrochemical systems. One of the reasons for this is that the surface of the nanostructures is insulated by stabilization compounds, which preserve the integrity of nanostructures but at the same time, form an insulating barrier for the charge transfer reactions.[13] One example is the OA and polymeric compounds produced in the course of the reaction. It is challenging to obtain access to the free or chemically functionalized and therefore organized surfaces for electrochemical systems.

We report on how we addressed this issue by assembling ultrathin gold nanowires and nanoparticles prepared by OA-based synthesis with a metalloprotein cyt *c* into a bioelectrochemically active nanoarchitecture for the first time. Key thermodynamic and kinetic

parameters of the direct electron transfer reaction of cyt c on these electrode surfaces were obtained. We demonstrate that oleylamine-stabilized gold nanostructures are prospective electrode materials for bioelectrochemical systems such as biosensors, bioelectronics, and energy research.

2. Experimental Section

2.1. Reagents and materials. Cytochrome c (horse heart, type VI), 6-mercaptohexanoic acid ($HS(CH_2)_5COOH$, 6-MHA), 2-mercaptoethanol (2-ME), ethanedithiol, oleylamine, AuCl, $HAuCl_4 \cdot 3H_2O$ were purchased from Sigma-Aldrich Chemicals and used as received. Distilled water was used for the experiments. Other chemicals were reagent grade.

2.2. Synthesis of gold nanostructures. Oleaylamine-based synthesis of gold nanoparticles was performed as described previously.[7] Gold nanowires were prepared by modification of procedure.[11] 200μL OA was mixed with 7.45 mg $HAuCl_4 \cdot 3H_2O$, 2.5 ml hexane was added followed by 100 μL of TIPS. After the reaction time of 5.5-6 h, the mixture was heated at 80 °C for about 15-30 sec. All samples were centrifugated and redispersed in hexane.

2.3. Electrode Preparation. To prepare thin-film gold working electrodes (WE), a silicon oxide layer of 1μm thickness was grown on a silicon substrate. Thin films of titanium (10 nm, adhesion layer) and gold (300 nm) were subsequently prepared on Si/SiO_2 substrates by sputter deposition. The electrodes were cleaned in acetone, propanol, and water followed by H_2O_2:H_2SO_4 1:2 v/v and water. The substrates were next subjected to electrochemical cleaning by consecutive potential cycles in 0.01 M KCl in 0.1 M H_2SO_4 between 0 and 1.5 V at 0.05 V s^{-1} starting and ending at 0 V vs. Ag/AgCl/KCl 3 M reference electrode). These electrodes are referred to as flat electrodes (without the immobilized nanostructures). Subsequently, various procedures were used to prepare the electrodes with nanostructured surfaces.

2.3.1. Flat thin-film electrodes. After electrochemical cleaning, the electrodes were immersed into 5 mM solutions of 6-MHA/2-ME (5mM/5mM) in hexane for 1 h. The electrodes were rinsed with hexane and phosphate buffer to eliminate excess alkanethiols. Cyt *c* was electrostatically adsorbed from 30 μM solutions in phosphate buffer (4.4 mM, pH 7.0, ionic strength 10 mM) at 4 ºC for 2 h. After adsorption, the substrates were thoroughly rinsed with phosphate buffer to remove any excess cyt *c* from the electrode surface.

2.3.2. Nanostructures immobilization via chemical binding (ED-NS electrodes). Either nanoparticles or nanowires were immobilized on the surface of the thin film gold electrodes via chemical binding with ethanedithiol (ED). After electrochemical cleaning as described above, the thin film substrates were immersed into 5 mM solution of ED in ethanol for 1 h. The substrates were rinsed with ethanol followed by hexane to eliminate excess ED. The samples of nanostructures were then dropped onto the surface of thin film gold electrodes from hexane solutions. The samples were left overnight to allow the nanostructures to adhere and were subsequently rinsed with hexane. When necessary, oxygen plasma treatment was used and the samples were subsequently rinsed with hexane. Preparation of carboxylate-terminated thiol SAMs and adsorption of cyt *c* was performed as described above for the flat electrodes.

2.3.3. Nanostructures immobilization (NS-electrodes). After electrochemical cleaning of the thin film gold electrodes, the samples of nanostructures were dropped onto the electrode surface from hexane solutions. The samples were left overnight to allow the nanostructures to adhere and were then processed as described above.

Oxygen plasma treatment was performed in a plasma oven (diener electronic), 200 Watt, 0.7 mbar. Structural characterization of the electrode surfaces was performed by scanning electron microscopy (Gemini 1550 VP, Carl Zeiss, Jena, Germany) and TEM analysis (FEI CM20

microscope operated at 200 kV, by drop casting of particle dispersions on copper grids coated with Formvar film).

2.4 Electrochemical measurements. Cyclic voltammograms (CV) were acquired in a three-electrode setup controlled by potentiostat (AUTOLAB). The three-electrode cell was composed of a gold working electrode, a coiled platinum-wire auxiliary (counter) electrode, and a Ag/AgCl reference electrode (3 M KCl, E^f = 0.210 V vs. NHE). The values of potentials are reported vs. Ag/AgCl reference electrode. The diameter of the working electrode in the electrochemical cell was 0.5 cm. Electrochemical experiments were performed at room temperature 21±1 ºC in deaerated solutions. Solutions were deaerated with argon and maintained under an argon stream during the measurements. Electron transfer rate constants were evaluated using Laviron's method.[14]

2.5. Correction of peak potential. The anodic and cathodic peak potentials of cyt *c* on nanostructured electrodes were corrected for the uncompensated ohmic potential drop due the solution resistance according to the equation: $E_p^{cor} = E_p^{CV} - I_p \cdot R_u$, where E_p^{CV} is the E_p value defined from the voltammogram and R_u is the uncompensated resistance.[15] Peak potentials corrected using this equation are shown in Table 1. Conductivity of 0.1 M solution of sulfuric acid was measured as about 20 $Ohm^{-1} \cdot cm^{-1}$. Therefore, the Ohmic potential drop for measurements in sulfuric acid (Figure 2A) was about 1 mV and was considered negligible.

2.6. Plieth' approximation. According to Plieth' approximation,[16] a negative shift in the redox potential of metal nanoparticles compared to the redox potential of the bulk is proportional to the reciprocal radius: $\Delta\varepsilon = 2\gamma v_M/(zFr)$, where γ is the surface energy, $\gamma_{Au}(25\ °C) = 1880$ erg cm^{-2}, and v_M is the molar volume, 10.21 $cm^3\ mol^{-1}$ and r is the radius of the nanoparticle.

2.7. Surface coverage of cyt *c*. For a redox couple that is immobilized on the electrode surface, the surface coverage on the electrode surface, Γ_o, is given by:

$$\Gamma_0 = \frac{A}{nF\mathrm{A}\upsilon},$$

where Γ_o is the surface coverage of cyt *c* on the electrode surface, *A* is the area under the peak (in units V·A), n is the number of electron transfer, A is the surface area of the flat electrode in the electrochemical cell (0.196 cm^2), and ν is the scan rate. The surface coverage was calculated from the baseline-corrected peaks. Theoretically, the crystallographic dimensions of cyt *c* of 2.6x3.2x3.0 nm yield approximately 20 pmol cm^{-2} for a close-packed monolayer of cyt *c*.[17]

3. Results and Discussion

The oleylamine-stabilized monodisperse nanoparticles (NPs) and ultrathin nanowires (NWs) used in our work were prepared by oleylamine synthesis,[7,11] drop-cast on the electrochemically cleaned gold thin film electrode surface. They were allowed to adhere overnight, were washed with hexane, and analyzed by electron microscopy, Figure 1 and Figures S1, S2A, S3A. The geometrical features of the nanostructures were as follows. The nanowires were about 2 nm in diameter and several hundreds of nanometers to micrometers in length, forming bundles, and the nanoparticles were 12 nm (9%) in diameter, Figure S1.

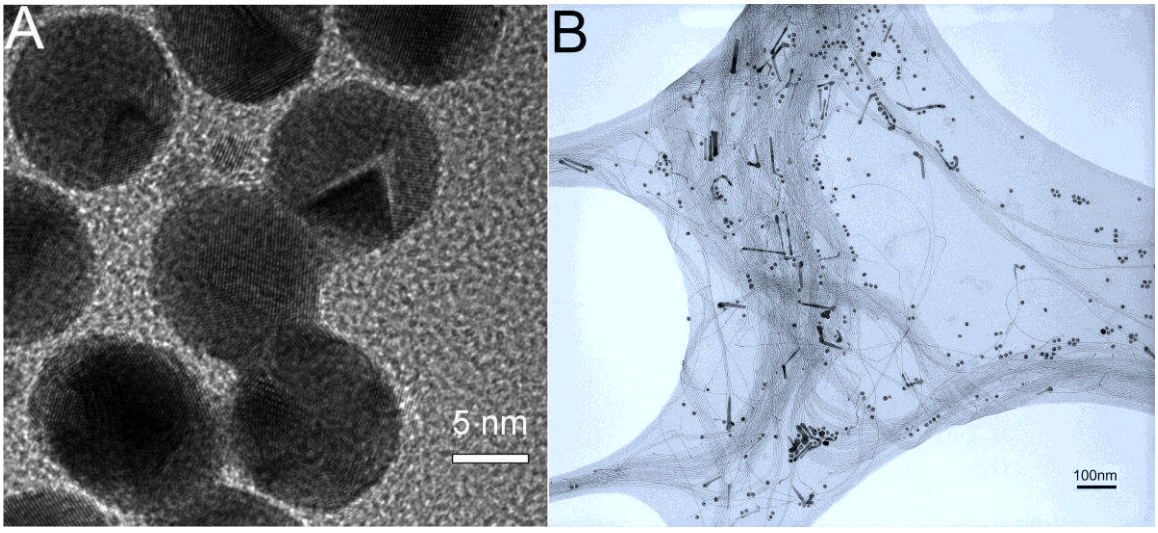

Figure 1. Transmission electron micrographs of (A) Au NPs and (B) Au NWs. Scale bars are 5 nm (Au NP) and 100 nm (Au NW).

3.1. Thermodynamic stability of OANWs. We observed that the NWs are not as stable as OANPs, which is in agreement with their large surface area and aspect ratio. In contrast to the OANPs, the OANWs are stable in hexane solutions for only about two weeks, they are disaggregated to nanoparticles after drying the solvent, prolonged exposure to ultrasound (Figure S2B), and are destroyed by prolonged exposure to oxygen plasma (OP) (Figure S2C). Using solvents interacting with the amino group of OA or Au(I) results in a partial or complete disaggregation of NWs (Figure S3).

Generally, we observed that the addition of polar solvent such as ethanol, which is widely used in the preparation and separation of nanostructures results in partial or complete disaggregation of NWs to NPs or nanorods. Figure S3 demonstrates such a case. The nanowires are observed in hexane-treated samples of nanostructures prepared according to [8], but mostly NPs were observed in the samples treated with ethanol. This is not unexpected, if we consider that the stabilizing effect of OA is based on the interactions $RH_2N\cdots Au(0)$ or $RH_2N\cdots Au(I)$ (tentatively assigned to a complex $[AuCl(RNH_2)]$ [18,19]), which have energies of about 44 kJ mol^{-1}.[20,21] The binding energy of these interactions is comparable with the binding energy of the hydrogen bond (5 to 30 kJ mol^{-1}, typically approx. 20 kJ mol^{-1}).[22] Therefore, hydrogen bonds such as $C_2H_5HO\cdots NH_2R$ can compete with amine-gold binding ($RH_2N\cdots Au(0)$ or $RH_2N\cdots Au(I)$) when ethanol is added. Moreover, if we accept that OA gold nanostructures are surrounded by Au(I)[18,19] (which attracts a stabilization shell of OA), then the role of ethanol is: 1) to distort or decrease the amount of stabilization OA molecules on the NS surface due to hydrogen bond formation, and 2) to reduce Au(I) to Au(0), while being oxidized to acetaldehyde,[23] thus also destabilizing the OA shell and

resulting in disaggregation of NWs. This implies that solvents which are able to interact either with Au(0) or Au(I) and form a hydrogen bond with the NH_2-group of OA would generally destabilize or disorder the stabilization shell and lead to a partial or complete disaggregation of NWs to NP, thereby increasing the NP/NW ratio. Thus, an OA stabilization shell is necessary to preserve the integrity of such energetically unfavorable ultrathin nanowire structures with a large surface area (aspect ratio up to 4000). Attempts to obtain access to the free surface of ultrathin nanowires may easily lead to their disaggregation into more stable nanostructures such as NPs or nanorods with lower surface energy (aspect ratio).

3.2. OANS on electrode surfaces. We employed two strategies to assemble the nanowires or nanoparticles on the thin-film gold electrodes (Scheme 1, see section 2.3 for details). In the first series (Scheme 1A), the nanowire or nanoparticles samples were allowed to adhere to the preliminarily cleaned planar gold film electrodes (NW-electrodes and NP-electrodes). In the second series (Scheme 1B), the planar electrodes were first modified with a homofunctional cross-linker ethaneditiol (ED) and the nanostructures were drop-cast on the thiol-functionalized electrode surface (ED-NW-electrodes and ED-NP-electrodes). Oleylamine stabilization molecules on the nanostructures surface are replaced by thiol molecules in this reaction. XPS surface analysis confirmed the formation of a sulfur-gold bond (see SI). The excess of OA was then removed by oxygen plasma (OP) treatment and hexane. The washing procedure removes the nanostructures not adhering to the electrode surface, so that the electrodes displayed patches of an exposed planar thin film gold surface (Figures S1, S2A, S3A)**.**

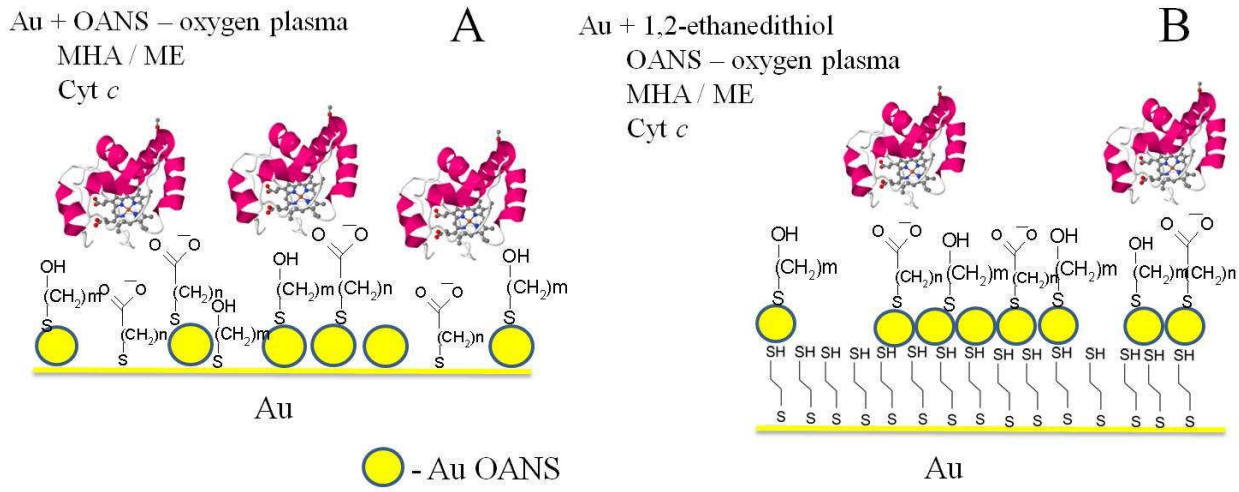

Scheme 1. Assembly of cyt *c* on electrodes (structure of horse heart cyt *c* is adapted from Protein Database, http://www.rcsb.org/pdb).

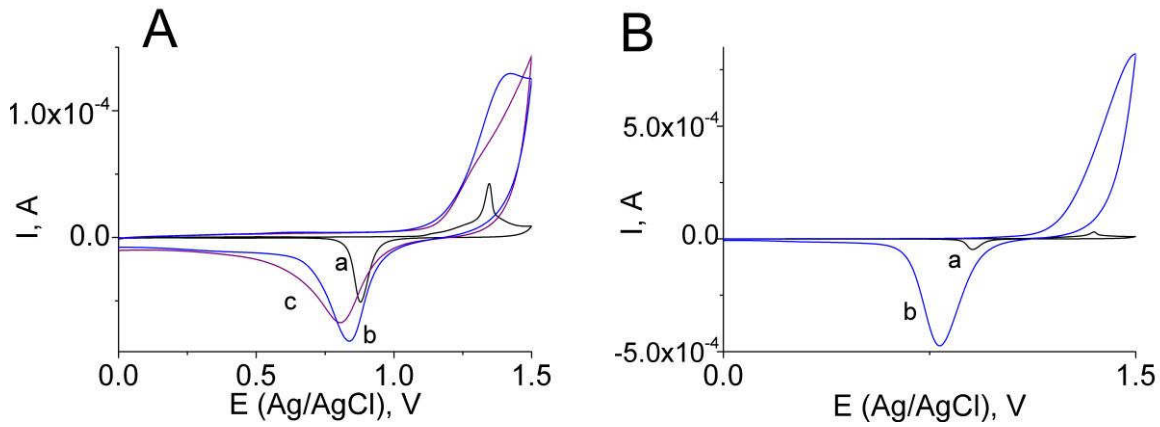

Figure 2. Oxidation and reduction of electrode surfaces in H_2SO_4, 0.1 M. (A) planar gold film (a), planar gold film modified with OANPs (b) and OANWs (c), scan rate - 30 $mV \cdot s^{-1}$; (B) planar gold film (a), modified with EDT-linked NWs (b), scan rate - 50 $mV \cdot s^{-1}$. OP treatment 5 min.

Electrodes modified with adhering (Scheme 1A) NPs and NWs demonstrated a negative shift of the reduction potential of gold compared to a bare film gold electrode of about -40 mV and -70 mV, respectively, Figure 2A (for the consideration of the Ohmic potential drop due to the solution resistance see section 2.5). The presence of OA on the surface, which was also oxidized

at high potentials, did not allow the gold oxidation potentials to be determined. In our discussion we consider a symmetric shift of the oxidation (E_a) and reduction (E_c) potentials of the reaction $Au^+ + e \rightarrow Au^0$, which are generally used to find a redox potential as $E'=(E_a+E_c)/2$. This observation correlates with theoretical and experimental studies that reported on the decreasing formal redox potential of metal nanoparticles with decreasing size and in comparison to that of the bulk metal.[16] The reason for the size-dependence of the electrochemical parameters of nanoparticles larger than a few angstroms in radius is the change of the Gibbs free energy associated with the change in the surface area (the Gibbs free energy of dispersion) and a shift of the Fermi level of the nanoparticles in comparison to the bulk metal.[24] In this sense, gold electrodes with adsorbed gold nanostructures of different sizes behave like "different metal electrodes" or electrodes with different standard potentials.[25] With respect to the electrochemical data reported so far, easier oxidation of metal nanoparticles (negative shift of anodic potentials) with decreasing nanoparticle size[26] and electrochemical Ostwald ripening[25] has been reported as a result of a negative shift of the standard potentials of smaller nanoparticles. Our data demonstrate that the reduction of the potential-determining ion, Au(I), on OANS electrodes proceeds at potentials more negative than for the planar metal electrode. According to Plieth' approximation (see section 2.6),[16] the gold nanoparticle of 12 nm in diameter would be composed of about 53347 gold atoms and would demonstrate a negative shift of redox potential of about -0.033 V with respect to the bulk gold. Since the redox potential determines the capability for reduction or oxidation, the negative shift of the redox potential can be considered as a reduced electron affinity of the gold nanostructures in comparison to the bulk metal.[25] The negative shift of the reduction potential of gold on nanostructured electrodes might also be influenced by different weights of the exposed gold plane surfaces, defects and edges due to the presence of the nanostructures. The effective electrode surface area of nanostructured assemblies

increased about 5.8 (S_{eff} = 1.15 ± 9% cm^2) and 6.2±12% (S_{eff} = 1.22± 14% cm^2) times compared to a planar gold electrode surface (S_{eff} = 0.196 ± 0.014 cm^2) for NP- and NW-electrodes, respectively, as it is calculated from the reduction peaks[27] (the measurements were performed in the electrochemical cell, where the geometrical surface area exposed to the electrolyte remains the same for all the electrodes). The data in Figure 2B also show that covalent binding of the nanostructures via a homofunctional cross-linker ED (Scheme 1B) increases the nanostructure density on the electrode surface (an increase of the effective surface area by about 20 times) but such an assembly, however, is not favourable for the electrochemistry of cyt *c* as it is shown below.

3.3. Electrochemistry of cyt *c*. Cyt *c* was immobilized on the nanoparticle or nanowire gold surfaces following the procedure adopted from Bowden et al.[28] (see Scheme 1 and section 2.3). In this immobilization method cyt *c* was electrostatically adsorbed on the negatively charged functional groups of mercaptocarboxylic acid.[2,29-32] It is supposed that electrostatic adsorption proceeds via interactions of the terminal amine groups of lysine amino acid residues close to the heme pocket (Lys-13, 72, and 86 of horse heart cyt *c* [30]), which are positively charged at neutral pH, with the negatively charged carboxylate surface of the electrodes. Weak interactions with the alcohol group of mercaptoethanol were also found for Lys-8, 13, and 27 of horse heart cyt *c*.[30] Since interactions which are responsible for binding cyt *c* to the thiol-functionalized electrodes are electrostatic in nature, the immobilization and electrochemical experiments were performed in a low ionic strength buffer (typically 1 to 10 mM ionic strength, 10 mM ionic strength buffer was used in a present work). Desorption of electrostatically immobilized cyt *c* upon exposure of the electrodes to the high ionic strength solutions was previously shown.[33] This effect can be explained by shortening the Debye length in high ionic strength solutions at which electrostatic interactions are reduced in strength (screened). The stability of the adsorbed electroactive cyt *c*

layer during experiments is also demonstrated in Figure S4 confirming that the protein doesn't diffuse into the solution. This result is in agreement with the previous results showing that the desorption of cyt *c* into electrolyte solutions from the carboxylate surface is negligible at low ionic strengths (< 50 mM phosphate buffer solution) in the pH range 6-9.[33,34]

Our experiments also confirmed an enhanced electrochemistry of cyt *c* on mixed thiol monolayers of mercaptocarboxylic acid-mercaptoalcohol in comparison with a single mercaptocarboxylic acid.[28] The linear dependence of the peak currents on the square root of the scan rate (Ip vs. $\nu^{1/2}$), Figure 3, confirmed the adsorption behavior, i.e. that electroactive cyt *c* was confined to the nanostructured surface.

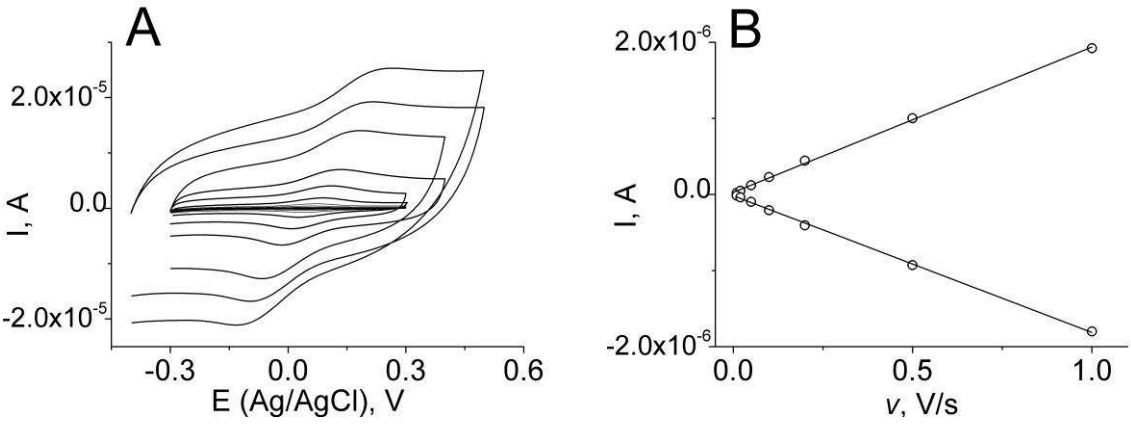

Figure 3. (A) Direct electron transfer of cyt *c* on the Au-NPs-SAM-cyt *c* electrodes, scan rate varies from 10 to 10000 mV s^{-1} (from inner to outer curve), PB 4.4 mM, pH 7.0. (B) Dependence of Ip on the scan rate for A confirms the adsorption behavior.

Figure 4A shows cyclic voltammograms (CVs) of cyt *c* on NS- (Scheme 1A) and ED-NS- (Scheme 1B) electrodes. For comparison, the CVs of a number of electrodes without immobilized cyt *c* are shown in Figure 4A and Figure S5. Mainly capacitive background currents are observed. The capacitive currents are larger for the NS-modified electrodes than for a flat electrode due to the increase of the effective surface area of the NS-modified electrodes. Redox

peaks of cyt *c* with better resolution were observed reproducibly on NS-electrodes as well as higher concentrations of electroactive cyt *c* on the electrode surface compared to those on ED-NS electrodes. This might be explained by the fact that in the case of adhering nanostructures (NS-electrodes), the areas of the planar electrode surface not covered with nanostructures would further react with negatively charged thiols (MHA-ME) introducing additional negative charges on the surface, thus favoring the electroactive orientation and conformation of cyt *c*.[29,34-37]

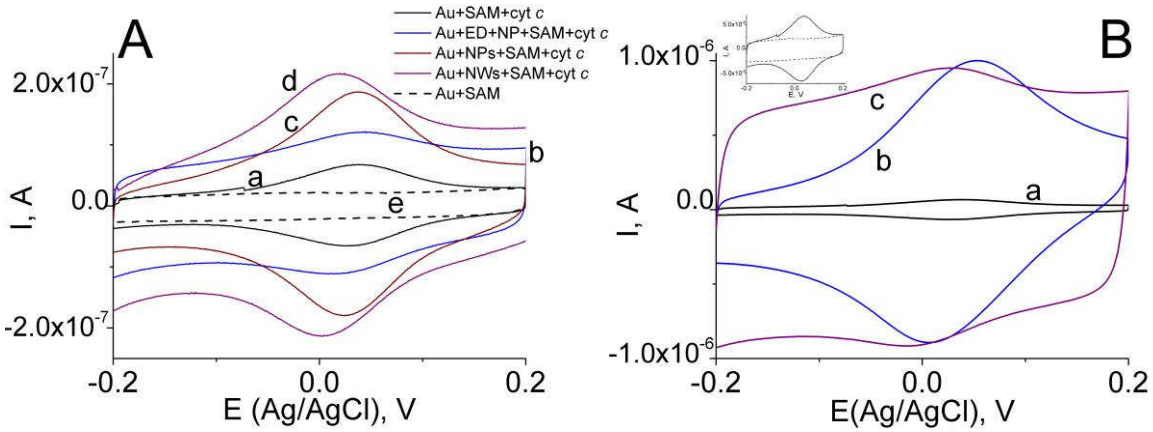

Figure 4. CVs of cyt *c* on electrodes: (A) OA replaced by thiols, (B) OA is additionally removed by oxygen plasma treatment before the reaction with thiols. In (A): planar thin-film Au-SAM-cyt *c* (a), Au-EDT-NPs-SAM-cyt *c* (b), Au-NPs-SAM-cyt *c* (c), Au-NWs-SAM-cyt *c* (d), Au-SAM (e, dashed line). (B): line (a) and insert in (B) show CVs of a planar thin film Au-SAM-cyt *c* electrode and Au-SAM electrode (dashed line) like lines (a) and (e) in (A), respectively, Au-NPs-OP_SAM-cyt *c* (b), Au-NWs-OP-SAM-cyt *c* (c). Other conditions: scan rate - 50 mV s-1, measurements were performed in 4.4 mM phosphate buffer, pH 7.0.

In our previous works, we observed that in the case of unfolding or denaturation of cyt *c* (e.g., as a result of unfavorable immobilization or constriction on the surface), an additional pair of redox peaks might appear at more negative potentials. These additional peaks can be assigned to the partly unfolded, denaturated or constrained fraction of cyt *c*. Axial ligands in cyt *c* are

methionine (a thioether side-chain group) and histidine (an imidazol side-chain group). The influence of axial ligands as well as protein structure on the redox potential, $E^{0'}$, of iron porphyrins has been shown.[38,39] Denaturation or constriction of the protein may result in a variation of the environment of the iron of the heme group of cyt *c*, thus producing a shift in the Fe(II/III) redox potential of cyt *c*. For example, with a help of the "tail porphyrin" concept it was shown that histidine replacement by methionine produced a shift of the redox potential of hemoproteins analogues of about 160 mV. Thus, one might expect the shift of the redox potential ($E^{0'}$) of cyt *c* and as a consequence an appearance of additional redox peaks due to removal of the axial ligand or increasing the distance between metal ion of the porphyrin and the axial ligands (e.g, as a result of denaturation or constriction on the surface). However, we did not observe these effects in the presented work.

Since electrochemical and XPS experiments showed that OA molecules were not completely replaced by thiols, we used OP treatment (5 min) to additionally remove OA from the surface. This treatment further enhanced the electrochemistry of cyt *c*, Figure 4B (NS-OP-electrodes) and Table 1. An increased amount of the immobilized electroactive cyt *c* is observed as well. This is probably due to the additional removal of the insulating organic molecule OA, which plays a role of an electron transfer barrier. As one can see from CVs (Figure 4), the NS-modified electrodes demonstrate larger background capacitive currents (this might be expected due to the increased surface area). Therefore, the redox peaks (Faradaic currents) of cyt *c* are poorly resolved on the NWs-modified electrodes.

Table 1 compares redox peak separation (ΔE), redox potentials (E'), heterogeneous electron transfer rate (k_{ET}) found by the Laviron method,[14] and concentrations of electroactive cyt *c* on the surface (Γ_o) (for the details see experimental section). Additionally, we used the Marcus equation

(1)[40] for the nonadiabatic first-order reaction to calculate the apparent electron transfer distance, d_{ET}:

$$k_{et}=\nu\cdot\exp[-\beta(d_{ET}-d_0)]\exp[-\Delta G^*/RT], \quad (1)$$

where ν is the frequency factor generally taken to be 10^{13} s^{-1},[41] β is the factor of decrease in the electron transfer rate with increasing distance (ca. 1 Å),[42] d_0 is the van der Waals contact distance, assumed to be 3 Å, and ΔG* is the free energy of activation.[40]

Table 1 Electrochemical characteristics of the heterogeneous electron transfer of cyt *c* on electrodes, Γ_o^{NS} / Γ_o^{flat} – ratio of concentrations of cyt *c* on the OANS-electrode and flat electrode[a].

Electrode system	E', mV	ΔE_{cor}, mV	k_{ET}^L, s^{-1}	d_{ET}^M, Å	Γ_o, pmol cm^{-2}	$\Gamma_o^{NS}/\Gamma_o^{flat}$
Au-SAM	34(2)	8(1)	9(1.1)	18(2)	5.3(0.3)	1
Au-NP-OP-SAM	32(4)	39(5)	2.0(0.3)	21(2.7)	94(8)	18
Au-NW-OP-SAM	12(6)	28(6)	2.4(0.5)	22.6(4)	31(6)	6

[a] E' – redox potential of cyt *c* taken as the average of the reduction and oxidation peak potentials, ΔEcor - difference between peak potentials corrected for the ohmic potential drop due to the solution resistance, k_{ET}^L – heterogeneous electron transfer constant found by the Laviron method, d_{ET}^M - an apparent electron transfer distance found using eq. (1), Γo – concentration of cyt *c* on the surface, 95 % confidence intervals are given in parenthesis. The electrochemical characteristics of cyt *c* on the electrodes reflect not only the averaged orientational populations of electroactive cyt *c* [35] but also the averaged nanostructured electrode surface.

We observed that the redox potential of the Fe(III/II) ferri/ferro-cyt *c* couple adsorbed on NS-OP-electrodes demonstrated a slight shift in the cathodic direction, see Table 1. This effect is most pronounced for NWs-OP-electrodes. The effect might be due to the different conformation and orientation of cyt *c* adsorbed on various surfaces.[29,34-37]

For basic and applied studies cyt *c* was immobilized on various flat and nanostructured surfaces, e.g., gold nanostructures (mostly gold nanoparticles)[6,43-48], graphene nanosheets[5] , and fullerene film modified electrodes[49]. The data on the thermodynamics and kinetics of interfacial redox processes of cyt *c* electrostatically adsorbed on the surfaces, however, reveal a large scattering of the data for the formal redox potential, $E^{0'}$, the heterogeneous electron transfer rate constant, k_{ET}, and the amount of the immobilized electroactive cyt *c*. For cyt *c* electorstatically adsorbed on SAMs of thiols values of $E^{0'}$ between -10 and 60 mV (vs. Ag/AgCl) have been reported[44,45] (the formal potential of native cyt *c* is about 70 mV vs. Ag/AgCl sat. KCl in a phosphate buffer solution of pH 7[50]). The heterogeneous electron transfer rate constant is within 0.3 – 880 s^{-1}.[34,44,46,51] The heterogeneous electron transfer rate constant decreases with the increase of the electron transfer distance (alkanethiol chain-length).[34] Moreover, it was shown that it was primarily the kind of the metal rather than its surface morphology (roughness) that controls the thermodynamics and kinetics of interfacial redox processes of electrostatically adsorbed cyt *c*.[52] Additionally, some discrepancy in the k_{ET} values may be explained by the observed dependence of k_{ET} on *v* (scan rate).[51] This dependence was attributed to electroactivity changes resulting from reorientation of molecules during the potential scan. The scan rate dependence of k_{ET} makes it difficult to compare the data for the heterogeneous electron transfer rate constant using Laviron's method for cases ΔE <200 mV and ΔE >200 mV.[14,51,52] It was demonstrated that gold nanoparticles coated with thiol-based SAMs catalyze interfacial electrochemical electron transfer of redox metalloproteins.[6,43,47] High surface coverage of cyt *c* up to about 123 pmol cm^2 in layered nanospace of grapheme nanosheets[2c] compared to the theoretical value of monolayer cyt *c* on the GCE surface 13 pmol cm^{-2} [5] and 20 pmol cm^{-2} [17] on the gold surface has been reported. Although, lower values of the electroactive coverage on SAM-modified flat gold electrodes are usually reported.

We found the energy of activation of the electron transfer reaction of immobilized cyt *c* from the temperature dependence of the electron transfer rate (Figure S6, Arrhenius plot). It is assumed that $E_a \cong \Delta H^*$,[40] where E_a was found from the Arrhenius plots. We further assume that the contribution of the entropy of activation to the free energy of activation ΔG^* of ET is negligibly small,[53,54] therefore, $\Delta G^* \cong \Delta H^*$. Table 2 compares the values of the activation energies of the heterogeneous electron transfer of cyt *c* on planar Au-SAM-cyt *c*, Au-NW-OP-SAM-cyt *c,* and Au-NP-OP-SAM-cyt *c*. The reorganization energies were estimated using Marcus theory, i.e. $\lambda = 4\Delta G^*$ [40,53] and are summarized in Table 2.

Table 2 Activation energies (Ea) and reorganization energies (λ) of the heterogeneous electron transfer of cyt c on electrodes[a].

Electrode system	E_a, kJ mol^{-1}	λ, eV
Au-SAM	31(3)	0.32
Au-NP-OP-SAM	28(3)	0.29
Au-NW-OP-SAM	23(4)	0.24

[a] 95 % confidence intervals are given in parenthesis.

The value of d_{ET} for the flat electrodes, which is calculated as 16.8 Å for MHA (using values of 1.16 Å per methylene unit (-CH_2-), 4.8 Å intercept,[55] and about 5 Å for the heme to edge distance in cyt *c* [53]) is in a good agreement with a d_{ET} of 18 Å (Table 1) found for the flat electrodes. On the other hand, the d_{ET}^M values for NS-electrodes deviate to a greater extent from the calculated 16.8 Å distance. We assume that some OA molecules remain between the gold thin film electrode surface and adhering nanostructures thus providing an additional tunneling barrier for the electron transfer. Indeed, the oleylamine molecules on the NW were found to be 1 - 2 layers

thick, and exhibited a thickness in the nanometer range, representing an isolating barrier for electron tunneling.[13] This explains deviations of the apparent electron transfer distance, d_{ET}^{M}, for the NS-electrodes (in Table 1, found from the Markus equation) from the calculated value of about 16.8 Å. Thus, additional electron transfer barrier between NPs and NWs and the electrode surface contributed to the k_{ET} found for Au-NP-OP-SAM-cyt *c* and Au-NW-OP-SAM-cyt *c* systems. Therefore, higher values of k_{ET} immediately between cyt *c* and thiol modified NPs and NWs are expected than those found for the electrode assembly. For the bundles of nanowires, the electron transfer process faces a longer path with more barriers on the interface, thus the wires' own contact resistance makes the transfer process slower. This may explain that the rate decreases while the energy of activation decreases.

4. Conclusions

In summary, we realized an assembly of ultrathin NWs and NPs prepared by OA-based synthesis with a metalloprotein in a bioelectrochemically active nanoarchitecture for the first time. The gold reduction potential of electrodes modified with ultrathin nanowires and nanoparticles demonstrated cathodic shift. We showed that the geometrical features of the nanostructures and the method of their assembly allow fine tuning of the electrochemical properties of the nanostructured gold electrode. Various methods of the bioelectronic circuit assembly of a metalloprotein and OANPs and OANWs are demonstrated and discussed. Nanoconjugates with OANSs covalently attached to the gold electrode surface demonstrate a lower performance in combination with a metalloprotein electrostatically adsorbed on the thiol functionalized gold surface compared to the systems with OANSs adsorbed on the electrode surface. Novel nanostructured electrodes provide a good environment for stable and

reproducible immobilization of the electroactive metalloprotein. While the concentration of the electroactive cyt *c* is drastically increased, studies on the surface treatment and immobilization of nanowires probably improve the kinetics of electron transfer in the Au-OANSs-SAM-cyt *c* assembly to further realize the potential of OA nanostructures for bioelectrochemical systems. The nanostructures prepared by oleylamine synthesis can prospectively be used to assemble other biomolecules into functional nanoarchitectures for sensors, artificial electron transport chains, metalloprotein electronics, and energy research.

ACKNOWLEDGMENT

We thank Dr. D. Mayer for helpful discussions, M. Banzet and E. Brauweiler-Reuters for preparation of the thin film gold electrodes and SEM imaging.

ASSOCIATED CONTENT

Supporting Information Available: SEM images of nanostructures (Figures S1 to S3), electrochemistry of cyt *c* on mixed thiol monolaeyers (Figures S4 and S5), XPS analysis (Table S1), Arrhenius plots for electron transfer in cyt *c* immobilized electrodes (Figure S6). This material is available free of charge via the Internet at http://pubs.acs.org.

AUTHOR INFORMATION

Corresponding Author

*Peter-Grünberg Institute-8, Forschungszentrum Jülich GmbH, 52428, Jülich and Jülich-Aachen Research Alliance (JARA_FIT). Tel: +49 2461612364; Fax: +49 2461618733; E-mail: y.mourzina@fz-juelich.de

Author Contributions

The manuscript was written through contributions of all authors. All authors have given approval to the final version of the manuscript. All authors contributed equally.

ABBREVIATIONS

OA, oleylamine; NS, nanostructures; NP, nanoparticles; NW, nanowires; ED, ethanedithiol; OANS, oleaylamine nanostructures; OP, oxygen plasma; SAM, self-assembled monolayer.

REFERENCES

1. Bartlett, P. N. *Bioelectrochemistry. Fundamentals, Experimental Techniques and Applications*; John Wiley & Sons: Wiltshire, 2008.

2. Fedurco, M. Redox Reactions of Heme-Containing Metalloroteins: Dynamic Effects of Self-Assembled Monolayers on Thermodynamics and Kinetics of Cytochrome *c* Electron-Transfer Reactions. *Coord. Chem. Rev.* **2000**, *209*, 263-331.

3. Nakashima, T.; Sano, M. Single-Walled Carbon Nanotube as 1D Array of Reacting Sites: Reaction Kinetics of Reduction of Cytochrome *c* in Tris Buffer. *J. Phys. Chem. C* **2011**, *115*, 20931-20936.

4. Lee, C. H.; Lang, J.; Yen, C. W.; Shih, P.C.; Lin, T. S.; Mou, C. Y. Enhancing Stability and Oxidation Activity of Cytochrome *c* by Immobilization in the Nanochannels of Mesoporous Aluminosilicates. *J. Phys. Chem. B* **2005**, *109*, 12277-12286.

5. Hua, B.Y.; Wang, J.; Wang, K.; Li, X.; Zhu, X. J.; Xia, X.H. Greatly Improved Catalytic Activity and Direct Electron Transfer Rate of Cytochrome *c* Due to the Confinement Effect in a Layered Self-Assembly Structure. *Chem. Comm*. **2012**, *48*, 2316-2318.

6. Jensen, P. S.; Engelbrekt, C.; Sørensen, K. H.; Zhang, J.; Chi, Q.; Ulstrup, J. Au-Biocompatible Metallic Nanostructures in Metalloprotein Electrochemistry and Electrocatalysis. *J. Mater. Chem.* **2012**, *22*, 13877-13882.

7. (a) Kisner, A.; Lenk, S.; Mayer, D.; Mourzina, Y.; Offenhäusser, A. Determination of the Stability Constant of the Intermediate Complex during the Synthesis of Au Nanoparticles Using Aurous Halide. *J. Phys. Chem. C* **2009**, *113*, 20143-20147.

8. Kisner, A.; Heggen, M.; Fernández, E.; Lenk, S.; Mayer, D.; Simon, U.; Offenhäusser, A.; Mourzina, Y. The Role of Oxidative Etching in the Synthesis of Ultrathin Single-Crystalline Au Nanowires. *Chemistry Eur. J.* **2011**, *17*, 9503-9507.

9. Aslam, M.; Fu, L.; Su, M.; Vijayamohanan, K.; Dravid, V.P. Novel One-Step Synthesis of Amine-Stabilized Aqueous Colloidal Gold Nanoparticles. *J. Mater. Chem.* **2004**, *14*, 1795-1797.

10. Halder, A.; Ravishankar, N. Ultrafine Single-Crystalline Gold Nanowire Arrays by Oriented Attachment. *Adv. Mater.* **2007**, *19*, 1854-1858.

11. Feng, H.; Yang, Y.; You, Y.; Li, G.; Guo, J.; Yu, T.; Shen, Z.; Wu, T.; Xing, B. Simple and Rapid Synthesis of Ultrathin Gold Nanowires, Their Self-Assembly and Application in Surface-Enhanced Raman Scattering. *Chem. Comm.* **2009**, *15*, 1984-1986.

12. Lu, X.; Yavuz, M. S.; Tuan, H. Y.; Korgel, B. A.; Xia, Y. Ultrathin Gold Nanowires Can Be Obtained by Reducing Polymeric Strands of Oleylamine-AuCl Complexes Formed via Aurophilic Interaction. *JACS*, **2008**, *130*, 8900-8901.

13. Pud, S.; Kisner, A.; Heggen, M.; Belaineh, D.; Temirov, R.; Simon, U.; Offenhäusser, A.; Mourzina, Y.; Vitusevich, S. Features of Transport in Ultrathin Gold Nanowire Structures. *Small* **2012**, *9*, 846-852.

14. Laviron, E. General Expression of the Linear Potential Sweep Voltammogram in the Case of Diffusionless Electrochemical Systems. *J. Electroanal. Chem.* **1979**, *101*, 19-28.

15. Neumann, J. Resistance for Flow of Current to a Disk. *J. Electrochem. Soc.* **1996**, 501.

16. Plieth, W. J. Electrochemical Properties of Small Clusters of Metal Atoms and Their Role in the Surface Enhanced Raman Scattering. *J. Phys. Chem.* **1982**, *86*, 3166-3170.

17. Willit, J. M.; Bowden, E.F. Adsorption and Redox Thermodynamics of Strongly Adsorbed Cytochrome *c* on Tin Oxide Electrodes. *J. Phys. Chem.* **1990**, *94*, 8241-8246.

18. Kumar, A.; Mandal, S.; Selvakannan, P. R.; Pasricha, R.; Mandale, A. B.; Sastry, M. Investigation into the Interaction between Surface-Bound Alkylamines and Gold Nanoparticles. *Langmuir* **2003**, *19*, 6277-6282.

19. Gomez, S.; Philippot, K.; Colliere, V.; Chaudret, B.; Senocq, F.; Lecante, P. Gold Nanoparticles from Self-Assembled Gold(I) Amine Precursors. *Chem. Comm.* **2000**, 1945-1946.

20. Halder, A.; Ravishankar, N. Ultrafine Single-Crystalline Gold Nanowire Arrays by Oriented Attachment. *Adv. Mater*. **2007**, *19*, 1854-1858.

21. Pong, B. K.; Lee, J. Y.; Trout, B. L. First Principles Computational Study for Understanding the Interactions between ssDNA and Gold Nanoparticles: Adsorption of Methylamine on Gold Nanoparticulate Surfaces. *Langmuir* **2005**, *21*, 11599-11603.

22. Atkins, P.; De Paula, J. *Physical Chemistry*; Wiley-VCH: Weinheim, 2006.

23. Ron, H.; Matlis, S.; Rubinstein, I. Self-Assembled Monolayers on Oxidized Metals. 2. Gold Surface Oxidative Pretreatment, Monolayer Properties, and Depression Formation. *Langmuir* **1998**, *14*, 1116-1121.

24. Henglein, A. Physicochemical Properties of Small Metal Particles in Solution: "Microelectrode" Reactions, Chemisorption, Composite Metal Particles, and the Atom-to-Metal Transition. *J. Phys. Chem*. **1993**, *97*, 5457-5471.

25. Redmond, P. L.; Hallock A. J.; Brus, L. Electrochemical Ostwald Ripening of Colloidal Ag Particles on Conductive Substrates. *Nano Lett.* **2005**, *5*, 131-135.

26. Ivanova, O. S.; Zamborini, F. P. Size-Dependent Electrochemical Oxidation of Silver Nanoparticles. *JACS* **2010**, *132*, 70-72.

27. Hoogvilet, J.C.; Dijksma, M.; Kamp, B.; van Bennekom, W.P. Electrochemical Pretreatment of Polycrystalline Gold Electrodes To Produce a Reproducible Surface Roughness for Self-Assembly: A Study in Phosphate Buffer pH 7.4. *Anal. Chem.* **2000**, *72*, 2016-2021.

28. Leopold, M. C.; Bowden, E. F. Influence of Gold Substrate Topography on the Voltammetry of Cytochrome *c* Adsorbed on Carboxylic Acid Terminated Self-Assembled Monolayers. *Langmuir* **2002**, *18*, 2239-2245.

29. (a) Chen, X.; Ferrigno, R.; Yang, J.; Whiteseides, G. M. Redox Properties of Cytochrome *c* Adsorbed on Self-Assembled Monolayers: A Probe for Protein Conformation and Orientation. *Langmuir* **2002**, *18*, 7009-7015.

30. Ataka, K.; Heberle, J. Functional Vibrational Spectroscopy of a Cytochrome *c* Monolayer: SEIDAS Probes the Interaction with Different Surface-Modified Electrodes. *J. Am. Chem. Soc*. **2004**, *126*, 9445-9457.

31. Murgida, D.H.; Hildebrandt, P. Heterogeneous Electron Transfer of Cytochrome *c* on Coated Silver Electrodes. Electric Field Effects on Structure and Redox Potential. *J. Phys. Chem*. *B* 2001, *105*, 1578-1586.

32. Feng, Z.Q.; Imabayashi S.; Kakiuchi, T.; Niki, K. Long-Range Electron-Transfer Reaction Rates to Cytochrome *c* across Long- and Short-chain Alkanethiol Self-Assembled Monolayers: Electroreflectance Studies. *J. Chem. Soc., Faraday Trans.* **1997**, *93*, 1367-1370.

33. Clark, R.A.; Bowden, E.F. Voltammetric Peak Broadening for Cytochrome *c*/Alkanethiolate Monolayer Structures: Dispersion of Formal Potentials. *Langmuir* **1997**, *13*, 559-565.

34. Avila, A.; Gregory, B. W.; Niki, K.; Cotton, T. M. An Electrochemical Approach to Investigate Gated Electron Transfer Using a Physiological Model System: Cytochrome *c*

Immobilized on Carboxylic Acid-Terminated Alkanethiol Self-Assembled Monolayers on Gold Electrodes. *J. Phys. Chem. B* **2000**, *104*, 2759-2766.

35. Araci, Z. O.; Runge, A. F.; Doherty, W. J. III; Saavedra, S. S. Correlating Molecular Orientation Distributions and Electrochemical Kinetics in Subpopulations of an Immobilized Protein Film. *JACS* **2008**, *130*, 1572-1573.

36. Murgida, D.H.; Hildebrandt, P. Redox and Redox-Coupled Processes of Heme Proteins and Enzymes at Electrochemical Interfaces**.** *Phys. Chem. Chem. Phys*. **2005**, *7*, 3773-3784.

37. Zhou, J.; Zheng, J.; Jiang, S. Molecular Simulation Studies of the Orientation and Conformation of Cytochrome c Adsorbed on Self-Assembled Monolayers. *J. Phys. Chem. B* **2004**, *108*, 17418-17424.

38. Mashiko, T. Marchon, J.C.; Musse, D.T.; Reed, C.A.; Kastner, M.; Scheidt, W.R. Cytochrome c Models. *Inorg. Chem*. **1979**, *18*, 3653-3655.

39. Kadish, K.M.; Smith, K.M.; Guilard, R. *The Porphyrin Handbook: Inorganic, Organometallic and Coordination Chemistry;* Academic Press: USA, 2000, V. 3.

40. Marcus, R.A.; Suttin, N. Electron Transfers in Chemistry and Biology. *Biochim. Biophys. Acta* **1985**, *811*, 265-322.

41. Marcus, R. The Second R. A. Robinson Memorial Lecture. Electron, Proton and Related Transfers. *Faraday Discuss. Chem. Soc.* **1982**, *74*, 7-15.

42. Gray, H. B.; Malström, B. G. Long-Range Electron Transfer in Multisite Metalloproteins. *Biochemistry* **1989**, *28*, 7499-7505.

43. Jensen, P.S.; Chi Q.; Grumsen, F.B.; Abad, J.M.; Horsewell, A.; Schiffrin, D. J.; Ulstrup, J. Gold Nanoparticle Assisted Assembly of a Heme Protein for Enhancement of Long-Range Interfacial Electron Transfer. *J. Phys. Chem C* **2007**, *111*, 6124-6132.

44. Reddy, K.K.; Gobi, K.V. Activated Direct Electron Transfer of NanoAu Biocongugates of Cytochrome *c* for Electrocatalytic Detection of Trace Levels of Superoxide Dismutase Enzyme. *Electrochim. Acta* **2012**, *78*, 109-114.

45. Liu, H.; Tian, Y.; Deng, Z. Morphology-Dependent Electrochemistry and Electrocatalytical Activity of Cytochrome *c. Langmuir* **2007**, *23*, 9487-9494.

46. Zhao, G.; Lei, Y.; Zhang, Y.; Li, H.; Liu, M. Growth and Favorable Bioelectrocatalysis of Multishaped Nanocrystal Au in Vertically Aligned TiO_2 Nanotubes for Hemoprotein. *J. Phys. Chem. C* **2008**, *112,* 14786-14795.

47. Caban, K.; Offenhaeusser, A.; Mayer, D. Electrochemical Characterization of the Effect of Gold Nanoparticles on the Electron Transfer of cytochrome *c*. *Phys. Status Solidi A* **2009**, *206*, 489-500.

48. Scanlon, M.D.; Salaj-Kosla, U.; Beloshapkine, S.; MacAodha, D.; Leech, D; Ding, Y.; Magner, E. Characterization of Nanoporous Gold Electrodes for Bioelectrochemical Applications. *Langmuir* **2012**, *28*, 2251-2261.

49. D'Souza, F.; Rogers, L.M.; O'Dell, E.S.; Kochman, A.; Kutner, W. Immobilization and Electrochemical Redox Behavior of Cytochrome *c* on Fullerene Film-Modified electrodes. *Bioelectrochemistry* **2005**, *66*, 35-40.

50. Dutton, P.L.; Wilson, D.E.; Lee, C.P. Oxidation-Reduction Potentials of Cytochromes in Mitochondria. *Biochemistry* **1970**, *9*, 5077-5082.

51. Willit, J.L.; Bowden, E.F., Determination of Unimolecular Electron Transfer Rate Constants for Strongly Adsorbed Cytochrome *c* on Tin Oxide Electrodes. *J. Electroanal. Chem*. **1987**, *221*, 265-274.

52. Millo, D.; Ranieri, A.; Gross, P.; Ly, H.K.; Borsari, M.; Hildebrandt, P.; Wuite, G.J.L.; Gooijer, G.; van der Zwan, G., Electrochemical Response of Cytochrome *c* Immobilized on

Smooth and Roughened Silver and Gold Surfaces Chemically Modified with 11-Mercaptounodecanoic Acid. *J. Phys. Chem. C* **2009**, *113,* 2861-2866.

53. Song, S.; Clark, R. A.; Bowden, E. F.; Tarlov, M. Characterization of Cytochrome *c*/Alkanethiolate Structures Prepared by Self-Assembly on Gold. *J. Phys. Chem*. **1993**, *97*, 6564-6572.

54. Weaver, J. M. Interpretation of Activation Parameters for Simple Electrode Reactions. *J. Phys. Chem*. **1976**, *80*, 2645-2651.

55. Bain, C. D.; Troughton, E. B.; Tao, Y. T.; Evall, J.; Whitesides, G.M.; Nuzzo, R. Formation of Monolayer Films by the Spontaneous Assembly of Organic Thiols from Solution onto Gold. *JACS* **1989**, *111*, 321-335.

GRAPHICAL ABSTRACT.